coatings

MDPI

Article

WC Decomposition Phenomena in ID-HVOF-Sprayed WC-CoCr Coatings Using Fine Powder Feedstock

Wolfgang Tillmann [1], Leif Hagen [1,*], Ingor Baumann [1] and Michael Paulus [2]

[1] Institute of Materials Engineering, TU Dortmund University, 44221 Dortmund, Germany; wolfgang.tillmann@tu-dortmund.de (W.T.); ingor.baumann@tu-dortmund.de (I.B.)
[2] Fakultät Physik/DELTA, TU Dortmund University, 44221 Dortmund, Germany; michael.paulus@tu-dortmund.de
* Correspondence: leif.hagen@tu-dortmund.de

Abstract: Over the last few decades, the high velocity oxygen fuel (HVOF) spraying of WC-CoCr for internal diameter (ID) coating has attracted much interest for hard chrome replacement. Current demands for the ID coating of small cylindrical parts necessitates the use of specialized spray gun equipment and powder feedstocks with small particle size fractions. Due to the limited spray distance inside cylindrical parts with small IDs, the process control, spraying fine WC-CoCr powders, meets new challenges to avoid significant WC decomposition, which increases the risk of mechanical degradation. Within the scope of this study, ID-HVOF spraying using a fine-structured WC-CoCr (−15 + 5 µm) feedstock with a mean WC particle size of 400 nm is examined with respect to the WC decomposition phenomena using X-ray diffraction (XRD). Hence, a statistical design of experiments (DoE) is utilized to systematically analyze various spray parameter settings along with their interaction as part of the WC to W_2C conversion.

Keywords: HVOF; WC-CoCr coatings; XRD

Citation: Tillmann, W.; Hagen, L.; Baumann, I.; Paulus, M. WC Decomposition Phenomena in ID-HVOF-Sprayed WC-CoCr Coatings Using Fine Powder Feedstock. *Coatings* **2022**, *12*, 124. https://doi.org/10.3390/coatings12020124

Academic Editors: Ludmila B. Boinovich and Devis Bellucci

Received: 1 December 2021
Accepted: 19 January 2022
Published: 23 January 2022

1. Introduction

Thermal spraying processes meet new challenges when it comes to the coating of inner surfaces of cylindrical components with small diameters, internal bore hole features, or hard-to-reach undercuts. Process limitations are mainly related to the perpendicularly directed particle spray jet used in thermal spraying processes, the large build-up of common spray guns, as well as the long stand-off distances required to ensure a sufficient heat and momentum transfer of spray particles. Over the last few decades, novel approaches in research and industry have focused on solving these problems by developing novel spray gun concepts for internal bore hole features, i.e., internal diameter (ID) applications. Due to the high kinetic energy of spray particles in high velocity oxy-fuel (HVOF) spraying, ID-HVOF spraying technology has great potential to deposit high wear resistant coatings. A conventional HVOF spray gun utilizes stand-off distances of 200 to 400 mm, which are simply not feasible given the limited accessibility of the ID of cylindrical parts unless the dimensions are quite large. To date, only a few studies have been conducted with regard to ID applications using ID-HVOF spraying systems, although such systems are already available for small IDs of up to 43 mm [1]. Current demands for ID coatings with small diameters require the use of a compact spray gun. The compact design is associated with a lower torch power, resulting in a reduced heat input into the spay particles at short stand-off distances. The use of a fine-structured feedstock, i.e., fine particle-sized spray powder, enables the sufficient heat and momentum transfer of spray particles even at short stand-off distances [1,2].

Agglomerated and sintered WC-Co(Cr) feedstocks commonly feature an agglomerate size distribution of −45 + 15 µm, with a mean value of their particle diameter larger than 20 µm. For non-optimized spray parameters, fine agglomerates (e.g., −10 + 2 µm,

−15 + 5 µm), including submicron-sized WC particles, tend to overheat during the spraying process, thus promoting undesirable phase transformation processes, such as oxidation and decarburization. Studying the microstructural characteristics of high velocity oxy-air fuel-sprayed WC-CoCr coatings derived from different agglomerated, sintered WC-CoCr powders (WC-CoCr agglomerate size/WC particle size: −30 + 5 µm/1−2 µm, −30 + 5 µm/200–400 nm, −15 + 5 µm/1–2 µm), Pulsford et al. [3] clarified that the WC decomposition strongly depends on the agglomerate size rather than the WC particle size. As reported in [4,5], WC decomposition phenomena predominantly lead to the formation of W_2C, and eta carbides such as $(W,Cr)_3Co_3C$, as well as Co(W,C). Here, WC is converted to W_2C and CO_2 at elevated temperatures in the presence of oxygen [6]. With regards to the mechanical coating properties, such phase transformation processes facilitate the formation of brittle areas within the coating, which thus implies a loss of the metallic character of the binder [5,7]. Consequently, the decomposition of WC can be detrimental to the wear resistance [8], thereby limiting the life span of the tribologically stressed surfaces.

In a previous study on ID-HVOF-sprayed WC-CoCr coatings, it was stated that the variation of the process parameters has a significant influence on the coating properties, such as porosity and hardness, but without addressing the microstructural properties [9]. Therefore, the correlation between the process parameters, affecting the heat and momentum transfer into the spray particles, and the atomic structure (phase formation) needs to be considered in more detail. In this study, WC-CoCr coatings derived from a fine-structured WC-CoCr (−15 + 5 µm) feedstock with a mean WC particle size of 400 nm, deposited by using an ID-HVOF spraying system, are examined with respect to the WC decomposition phenomena using XRD. A statistical approach (design of experiments, DoE) is utilized to systematically analyze various process parameter settings, along with their interaction on the resulting WC decomposition phenomena in the thus-produced WC-CoCr coatings.

2. Materials and Methods

2.1. Substrate and Feedstock Material

In preparation for the thermal spray experiments, rectangular (50 mm × 70 mm × 10 mm) C45 steel (1.0503; 258 ± 4 HV0.3) specimens were employed as substrates. The substrate surfaces were grit-blasted with corundum (grit size: F100 according to the Federation of European Producers of Abrasives, FEPA) using a blasting pressure of 0.5 MPa, a blasting angle of 45°, and an SOD of 100 mm. The grit-blasted substrates were afterwards cleaned in an ultrasonic ethanol bath for ten minutes. For the spraying experiments, an agglomerated, sintered WC-CoCr 86 10 4 powder served as the feedstock. According to the manufacturer, the WC-CoCr feedstock exhibits a WC Fisher sub-sieve size of 0.4 µm. As verified by laser light scattering (particle analyzer type S3500, Microtrac, York, PA, USA), the feedstock features a DP50 (50th percentile of diameter) of 10.43 µm for the volumetric particle size distribution, whereas the DP10 and DP90 are 6.83 and 16.89 µm, respectively.

2.2. Spraying Experiments

Within this study, the ID-HVOF spraying system IDCoolFlow Mono with the CPF2-Twin powder feeder system (Thermico, Dortmund, Germany) was utilized in order to conduct the spraying experiments. The spray gun was mounted on an industrial robot (type IRB4600/60, ABB, Zürich, Switzerland) to ensure a robot-controlled movement within the experiments.

Five independent variables were incorporated in a central composite design (CCD [10]), with 27 runs, including a single center run. Two center runs were added to the design in order to reduce the residual variance of the model. In terms of the CCD, the kerosene level (KL), oxygen level (OL), powder feeding rate (PFR), stand-off distance (SOD), and track pitch (TP) of the meander-shaped spray path were set as independent variables (Figure 1).

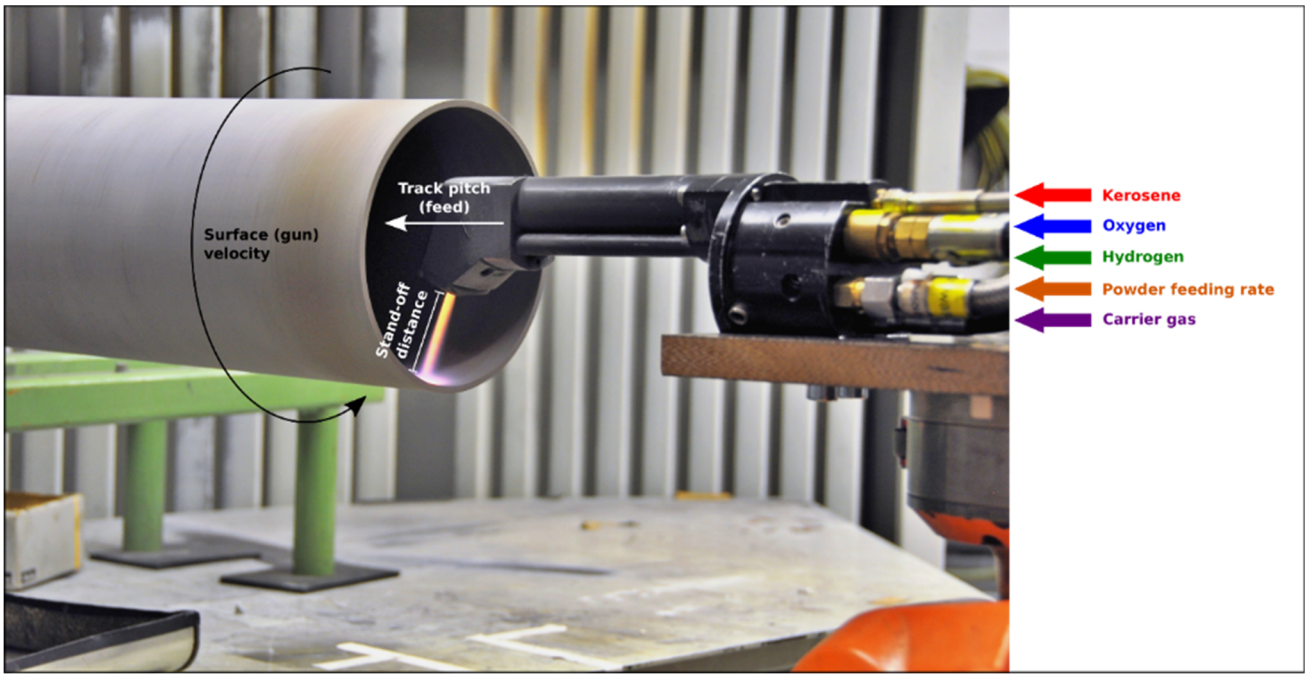

Figure 1. ID HVOF spraying process with relevant influencing parameters.

The level settings of the independent variables were converted to −1 (low), 0 (center), and +1 (high), whereas the so-called star points, $-\alpha$ and α, were converted to −1.664 and 1.664 to compute orthogonality within the CCD. The hydrogen level, the backside cooling pressure, as well as the handling parameters, such as the spray angle, gun velocity, and amount of overruns, were kept constant. The spray parameter settings are summarized in Table 1. The coatings thus produced had a thickness in the range of 195.6 ± 5.9 µm to 498.9 ± 9.9 µm, as well as a surface roughness depth Rz in the range of 18.6 ± 1.4 µm to 23.2 ± 1.8 µm, depending on the spray parameters. An analysis of the samples' cross-sections showed that the samples did not differ significantly on a mesoscopic length scale (data not shown).

Table 1. Spray parameter settings used within this study.

Independent Variables	**Central Composite Design**				
	−1.664	**−1**	**0**	**+1**	**1.664**
KL (l/h)	2.87	3.4	4.2	5.0	5.53
OL (l/min)	220.07	240	270	300	319.93
SOD (mm)	58.36	65	75	85	91.64
PFR (g/min)	26.68	30	35	40	43.32
TP (mm)	2.33	2.50	2.75	3.00	3.17
Constant Parameters					
Spray angle (°)	90	Hydrogen level (l/min)			70
Gun velocity (mm/s)	30.000	Backside cooling pressure (psi)			30
Overruns	25 passes	Powder carrier gas flow (l/min)			10

In terms of the statistical analysis, the WC decomposition expressed by the W_2C to WC ratio was set as the response variable. Here, the formation of W_2C by the coating process was monitored by integrating the intensities of the W_2C (112) Bragg reflections, which were normalized to the intensities of the WC reflections. Due to the small amounts of W_2C and the superposition of reflections from different eta phases, a conventional phase analysis via a fit of the entire diffractogram could not be performed. Therefore, the choice fell on the integration of the W_2C (112) Bragg reflection as a measure of W_2C

formation, since this reflection is isolated from the scattering contributions of other phases. Statistically significant influencing factors and factor combinations were determined by means of significance tests of the null hypothesis H_0, as demonstrated in [11]. Hence, p-values were calculated based on a t-distribution with $n - 1$ degrees of freedom (where n is the number of experiments) according to the t-statistic. Within this study, the significance level was set to 10% ($\alpha = 0.1$).

2.3. Analytic Methods

The phase composition of the WC-CoCr feedstock and the ID-HVOF-sprayed WC-CoCr coatings were determined by means of X-ray diffraction (XRD). The XRD experiments were carried out at the beamline BL9 [12] and BL2 at DELTA (Dortmund Electron Accelerator, Dortmund, Germany) using synchrotron radiation with an incident photon energy of 27 keV (BL9, wavelength $\lambda = 0.4592$ Å) and 12 keV (BL2, wavelength $\lambda = 1.033$ Å). The beam size was 0.2 mm × 1.0 mm (v × h) and the angle of incidence was set to 5 degrees, while the feedstock powder was measured in transmission geometry. For the detection of the scattered intensity, a MAR345 image plate detector (marXperts, Norderstedt, Germany) was used. A silicon powder sample was used for the calibration of the setup. Afterwards, the diffraction patterns were generated from the MAR images by using a FIT2D program package [13]. For the purpose of better comparability, the XRD spectra were converted to a photon energy of 8 keV. The phase analysis was performed with the program package Match! (CRYSTAL IMPACT, Bonn, Germany).

To evaluate the fracture toughness K_{IC} and the Vickers microhardness of the WC-CoCr coatings, Vickers indentations were applied to the polished cross-sections. The Vickers microhardness was measured according to the ASTM standard C1327, with a load of 2.942 N, using the M400 hardness tester (Leco, Mönchengladbach, Germany). Regarding the fracture toughness measurements for K_{IC}, the indentations were performed with a load of 49.03 N using the universal hardness tester DIA-TESTOR 7521 (Otto Wolpert Werke, Ludwigshafen, Germany). The crack lengths were evaluated using the light microscope AXIOPHOT with integrated software (Carl Zeiss, Jena, Germany). The fracture toughness K_{IC} was calculated according to Shetty and Wright [14]. For both the Vickers microhardness and the fracture toughness K_{IC}, five indents per coating were taken into account to calculate the mean value.

3. Results and Discussion

Figure 2 shows the XRD data of the different samples in an angular range in which the reflexes of the eta phases and the W_2C appear in addition to the strong WC reflections.

XRD analyses verify that the WC-CoCr feedstock (black line in Figure 2) is mainly composed of WC and Co, as well as some traces of Co_3W_3C. The XRD patterns obtained from the WC-CoCr coatings indicate the occurrence of WC, W_2C (or $W_2C_{0.84}$), and Co_3W_3C, while the intensity of the Co reflections, clearly visible in the feedstock diffractogram, is strongly reduced. In addition to the evolution of the Bragg reflections of the W_2C phase and the reduction of the Co signal, an increase in the scattering intensity is observed in an angular range between 40° and 45°, indicating the formation of amorphous or nanocrystalline phases. In general, a scattering of the measured data in the considered angular range can be observed for the different coatings, which can be explained by a different degree of W_2C formation. To obtain a more detailed overview of the dependence of the W_2C formation on the different process parameters, the correlation between the intensities of the W_2C (112) reflections normalized to the WC intensities and the variation of the process parameters was analyzed.

Table 2 summarizes the factor levels of the independent variables, as well as the corresponding results for the response variable, i.e., W_2C to WC ratio, taken from the peak analyses. The statistical design allows us to estimate the linear (L) and quadratic (Q) effects, and also the interactions (int.) between the variables.

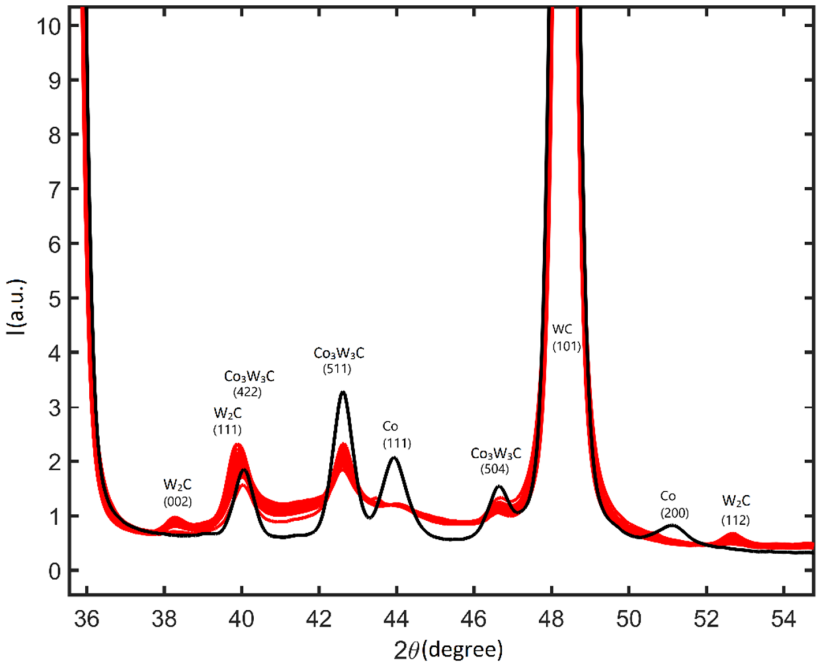

Figure 2. XRD patterns obtained from the WC-CoCr feedstock and 29 produced WC-CoCr coatings. Compared to the feedstock (black curve), the coatings (red curves) show a varying proportion of eta phases and W_2C, while the cobalt proportion decreases significantly.

Table 2. Level settings of the independent variables examined in the CCD with additional center run, and the corresponding response variable (mean values).

Run	KL (l/h)	OL (l/min)	SOD (mm)	PFR (g/min)	TP (mm)	I(W_2C)/I(WC)
1	1	1	−1	−1	1	0.0320
2	−1	1	−1	1	1	0.0313
3	0	0	0	0	1.664	0.0327
4	1	1	−1	1	−1	0.0356
5	−1	−1	1	1	1	0.0337
6	1	1	1	−1	−1	0.0327
7	0	−1.664	0	0	0	0.0401
8	−1	−1	1	−1	−1	0.0369
9	−1	1	1	1	−1	0.0338
10	−1	1	1	−1	1	0.0326
11	1	−1	1	−1	1	0.0390
12	−1	1	−1	−1	−1	0.0322
13	−1.664	0	0	0	0	0.0329
14	1	−1	1	1	−1	0.0337
15	0	0	0	0	−1.664	0.0332
16	1	−1	−1	−1	−1	0.0316
17	0	0	−1.664	0	0	0.0330
18	1	1	1	1	1	0.0313
19	1	−1	−1	1	1	0.0372
20	0	0	1.664	0	0	0.0374
21	1.664	0	0	0	0	0.0397
22(C)	0	0	0	0	0	0.0351
23	−1	−1	−1	−1	1	0.0391
24	0	0	0	1.664	0	0.0333
25(C)	0	0	0	0	0	0.0357
26	0	0	0	−1.664	0	0.0338
27(C)	0	0	0	0	0	0.0327
28	−1	−1	−1	1	−1	0.0329
29	0	1.664	0	0	0	0.0282

Table 3 shows the effect estimates and the *p*-values for the W_2C to WC ratio. The independent variables affect the response variable positively or negatively, which is shown by the sign of the effect estimate. The significant effects for $\alpha = 0.1$ are marked in bold.

Table 3. Effect estimates and *p*-values ($\alpha = 0.1$) for the CCD.

Independent Variable	I(W_2C)/I(WC)	
	Est.	***p*-Value ($\times 10^{-4}$)**
Mean/Interc.	**0.0346**	**0.0**
KL (L)	0.0011	3280.2
KL (Q)	0.0012	3864.5
OL (L)	**−0.0039**	**59.9**
OL (Q)	−0.0004	7590.7
SOD (L)	0.0008	4482.3
SOD (Q)	0.0004	7829.1
PFR (L)	−0.0007	5341.6
PFR (Q)	−0.0008	5268.2
TP (L)	0.0006	6160.8
TP (Q)	−0.0013	3439.6
KL * OL (int.)	0.0003	7836.6
KL * SOD (int.)	−0.0002	9061.4
KL * PFR (int.)	0.0015	2732.6
KL * TP (int.)	0.0006	6257.9
OL * SOD (int.)	−0.0004	7538.7
OL * PFR (int.)	0.0015	2732.6
OL * TP (int.)	**−0.0026**	**658.3**
SOD * PFR (int.)	−0.0014	3052.8
SOD * TP (int.)	−0.0010	4517.5
PFR * TP (int.)	−0.0015	2657.0

As shown in Table 3, the effect estimates reveal that the independent variable OL (L), as well as the interaction OL * TP (int.), have the most statistically significant effects on the W_2C to WC ratio. Here, OL (L) shows a p-value of 59.9×10^{-4}, whereas OL * TP (int.) exhibits a *p*-value of 658.3×10^{-4}. According to the effect estimates, an increased OL (L) and OL * TP (int.) leads to a reduced W_2C to WC ratio. This can be seen clearly in a comparison of the diffraction patterns. Here, for an increased OL as well as OL and TP, a reduced amount of W_2C with a simultaneously increased amount of Co_3W_3C, derived from the feedstock, can be obtained from the XRD patterns (Figure 3).

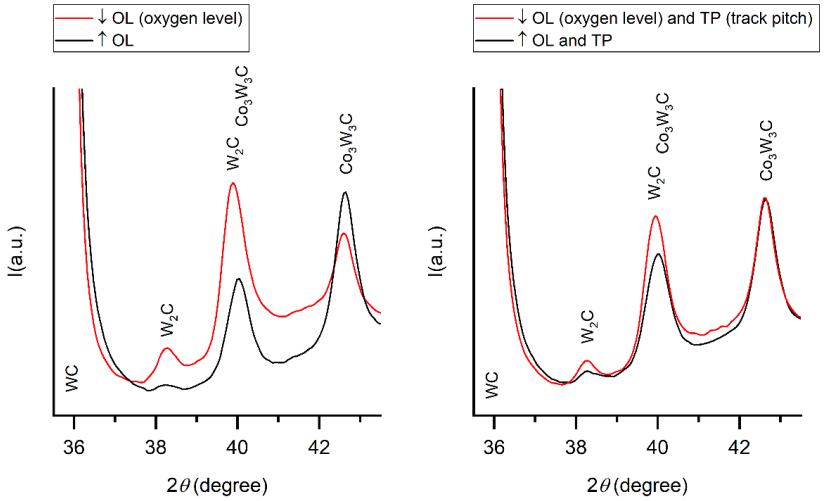

Figure 3. XRD pattern obtained from the produced WC-CoCr coatings using different spray parameter settings.

It is striking that the independent variables KL and SOD (known to be significant influencing factors on the heat and momentum transfer of spray particles in HVOF spraying [15]) exhibit no statistically significant effect, neither linear (L) nor quadratic (Q), on the W_2C to WC ratio. It is assumed that this is due to the fact that the WC-CoCr coatings produced within the boundaries of the spray parameter settings, in particular for the fine-structured WC-CoCr feedstock, predominantly lead to the formation of W_2C (Figure 4). This assumption is strengthened by the fact that a major amount of the interface of the polygonal-shaped WC particles (bright phase) to the surrounding Co-rich matrix (dark phase) is characterized by globular clusters (Figure 4b). It is very likely that W_2C developed directly from the decarburization of WC, as well as from the WC dissolved into the Co binder phase to form Co_3W_3C.

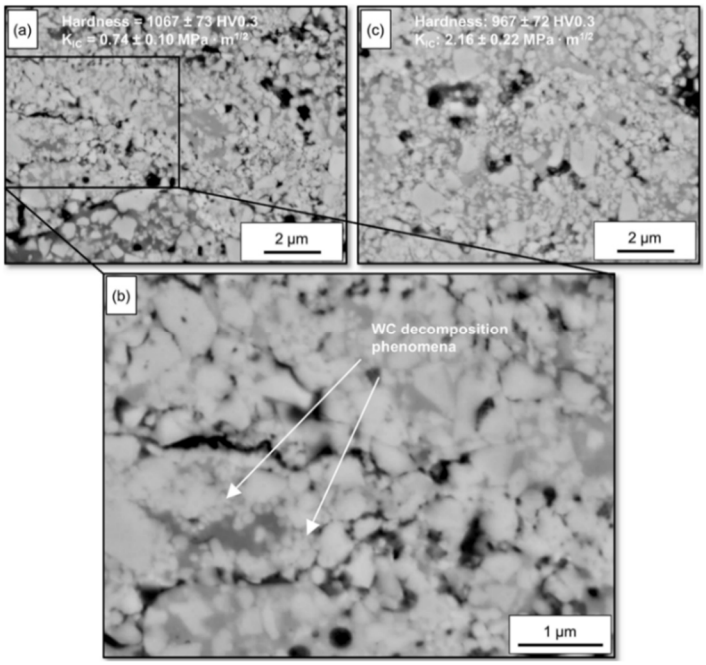

Figure 4. SEM images taken at the cross-section showing the BSE imaging of different WC-CoCr coatings: (**a**,**b**) using a decreased oxy-fuel ratio, and (**c**) using an increased oxy-fuel ratio. A certain number of polygonal-shaped WC particles changed into globular clusters.

Due to the inherent process characteristics of HVOF spraying, the spray particles are still undergoing heating when they impact the substrate or the previously deposited sublayers. At very short stand-off distances, combined with low traverse velocities of the spray torch moving over the substrate being coated, the heat input from the spray plume into the previously deposited spray particles or sublayers is higher than at longer stand-off distances [16]. Thus, the increased OL in the over-stoichiometric domain, as well as the adapted robot pathway (i.e., increased TP), are very likely to reduce the heat input into the previously deposited spray particles or sublayers. As a result, WC decomposition phenomena emerge less often. Chivavibul et al. [17] stated that the degree of decarburization in HVOF-sprayed WC–Co coatings represents a distinct influencing factor on the mechanical properties, such as fracture toughness K_{IC}. The authors demonstrated that the fracture toughness K_{IC} decreased with increased decarburization. With regard to the WC-CoCr coating systems thus produced, it can be seen that the fracture toughness K_{IC} is remarkably low compared with those observed for HVOF-sprayed WC-CoCr coatings [18–20]. Simultaneously, for a slightly increased fracture toughness K_{IC}, the Vickers indentation tests show a relatively low microhardness. In contrast, an increased microhardness can be observed with a simultaneously low fracture toughness K_{IC}.

4. Conclusions

The formation of W_2C in coatings has a significant effect on macroscopic coating properties, such as fracture toughness and hardness. Consequently, in this work, the formation of W_2C via the thermal decomposition of WC in WC-CoCr coatings as a function of various spray parameter settings, such as kerosene level, oxygen level, stand-off distance, powder feed rate, and track pitch, was investigated using XRD. For this purpose, a fine-structured WC-CoCr feedstock with an agglomerate size of −15 + 5 µm and a mean WC particle size of 400 nm was applied. Compared to the feedstock, it was shown that the amount of W_2C in the coatings increased significantly, while the scattering contributions of other eta phases, such as Co_3W_3C, did not increase. This result is comparable to the study of Pulsford et al., in which the formation of W_2C was also mainly observed for WC-CoCr coatings using a feedstock with the same agglomerate size of −15 + 15 µm, though with a WC particle size in the range of 1 to 2 µm. A statistical design of experiments (DoE) was utilized to systematically compare the different coatings and correlate the process parameters with the W_2C formation. It is shown that it is predominantly the oxygen level, as well as the interaction between the oxygen level and the track pitch, that creates the most statistically significant effects. An increased OL (L) and OL * TP (int.) leads to a reduced W_2C to WC ratio. The variation of the other spray parameters shows a non-vanishing but smaller effect on the formation of W_2C.

Author Contributions: Conceptualization, L.H.; investigation, L.H. and M.P.; writing—original draft preparation, L.H., I.B. and M.P.; writing—review and editing, L.H., I.B. and M.P.; supervision, W.T.; project administration, L.H.; funding acquisition, W.T. All authors have read and agreed to the published version of the manuscript.

Funding: The results have emerged within the framework of the IGF Project No. 19.914 N, with the subject of "Untersuchung der Einflussgrößen und prozess-technischen Randbedingungen auf die Schichtqualität beim Beschichten von rotationssymmetrischen Innenflächen mittels HVOF/HVAF". We thank the research association "Forschungsvereinigung Schweißen und verwandte Verfahren des DVS" and the Federation of Industrial Research Associations (AiF) for the promotion. The project was funded by the German Ministry of Economic Affairs and Energy via AiF within the framework of joint industrial research (IGF).

Institutional Review Board Statement: Not applicable.

Informed Consent Statement: Not applicable.

Data Availability Statement: Data sharing is not applicable to this article.

Acknowledgments: The authors acknowledge financial support by Deutsche Forschungsgemeinschaft and Technische Universität Dortmund/TU Dortmund Technical University within the funding programme Open Access Costs. The authors gratefully acknowledge the DELTA machine group for providing the synchrotron radiation.

Conflicts of Interest: The authors declare no conflict of interest.

References

1. Matthäus, G. Applications for HVOF and plasma coatings based on ultra-fine powder <10 µm. In Proceedings of the 11. HVOF Kolloquium, Erding, Germany, 25–26 October 2018; pp. 73–83.
2. Gutleber, J.; Molz, R.; He, J.; Weber, C.; Colmenares, J. New developments in HVOF spraying for internal diameter coatings. In Proceedings of the International Thermal Spray Conference, Düsseldorf, Germany, 7–9 June 2017; pp. 501–504.
3. Pulsford, J.; Kamnis, S.; Murray, J.; Bai, M.; Hussain, T. Effect of particle and carbide grain sizes on a HVOAF WC–Co–Cr coating for the future application on internal surfaces: Microstructure and wear. *J. Therm. Spray Technol.* **2018**, *27*, 207–219. [CrossRef]
4. Yuan, J.; Zhan, Q.; Huang, J.; Ding, S.; Li, H. Decarburization mechanisms of WC–Co during thermal spraying: Insights from controlled carbon loss and microstructure characterization. *Mater. Chem. Phys.* **2013**, *142*, 165–171. [CrossRef]
5. Berger, L.M. Hardmetal coatings—History and perspective. In Proceedings of the 11. HVOF Kolloquium, Erding, Germany, 25–26 October 2018; pp. 93–100.
6. Guilemany, J.M.; De Paco, J.M.; Miguel, J.R.; Nutting, J. Characterization of the W_2C phase formed during the high velocity oxygen fuel spraying of a WC+ 12 pct Co powder. *Metall. Mater. Trans. A* **1999**, *30*, 1913–1921. [CrossRef]

7. Gries, B. HVAF- Chance and challenge for users and for powder producers. In Proceedings of the 11. HVOF Kolloquium, Erding, Germany, 25–26 October 2018; pp. 57–72.
8. Shipway, P.H.; McCartney, D.G.; Sudaprasert, T. Sliding wear behaviour of conventional and nanostructured HVOF sprayed WC–Co coatings. *Wear* **2005**, *259*, 820–827. [CrossRef]
9. Tillmann, W.; Schaak, C.; Hagen, L.; Dildrop, M. Investigation of HVOF-ID spraying with WC-CoCr −15 +5 µm feedstock powder. In *IOP Conference Series: Materials Science and Engineering*; IOP Publishing: Bristol, UK, 2019; Volume 480, p. 012008.
10. St-Pierre, N.R.; Weiss, W.P. Technical note: Designing and analyzing quantitative factorial experiments. *J. Dairy Sci.* **2009**, *92*, 4581–4588. [CrossRef] [PubMed]
11. Tillmann, W.; Vogli, E.; Baumann, I.; Kopp, G.; Weihs, C. Desirability-based multi-criteria optimization of HVOF spray experiments to manufacture fine structured wear-resistant $75Cr_3C_2$–25(NiCr20) coatings. *J. Therm. Spray Technol.* **2010**, *19*, 392–408. [CrossRef]
12. Krywka, C.; Paulus, M.; Sternemann, C.; Volmer, M.; Remhof, A.; Nowak, G.; Nefedov, A.; Pöter, B.; Spiegel, M.; Tolan, M. The new diffractometer for surface X-ray diffraction at beamline BL9 of DELTA. *J. Synchrotron Rad.* **2006**, *13*, 8–13. [CrossRef] [PubMed]
13. Hammersley, A.P. FIT2D: An Introduction and Overview, ESRF Internal Report, ESRF97HA02T. 1997. Available online: https://www.esrf.fr/computing/scientific/FIT2D/FIT2D_INTRO/ (accessed on 30 November 2021).
14. Shetty, D.K.; Wright, I.G. On estimating fracture toughness of cemented carbides from Palmqvist crack sizes. *J. Mater Sci. Lett.* **1986**, *5*, 365–368. [CrossRef]
15. Baumann, I. Hochverschleißfeste und konturnahe Werkzeugoberflächen durch Hochgeschwindigkeitsflammspritzverfahren. Ph.D. Thesis, TU Dortmund University, Dortmund, Germany, 2012.
16. Katranidis, V.; Gu, S.; Allcock, B.; Kamnis, S. Experimental study of high velocity oxy-fuel sprayed WC–17Co coatings applied on complex geometries. Part A: Influence of kinematic spray parameters on thickness, porosity, residual stresses and microhardness. *Surf. Coat. Technol.* **2017**, *311*, 206–215. [CrossRef]
17. Chivavibul, P.; Watanabe, M.; Kuroda, S.; Shinoda, K. Effects of carbide size and Co content on the microstructure and mechanical properties of HVOF-sprayed WC–Co coatings. *Surf. Coat. Technol.* **2007**, *202*, 509–521. [CrossRef]
18. Giolli, C.; Turbil, M.; Rizzi, G.; Rosso, M.; Scrivani, A. Wear resistance improvement of small dimension invar massive molds for CFRP components. *J. Therm. Spray Technol.* **2009**, *18*, 652–664. [CrossRef]
19. Varis, T.; Suhonen, T.; Ghabchi, A.; Valarezo, A.; Sampath, S.; Liu, X.; Hannula, S.P. Formation mechanisms, structure, and properties of HVOF-sprayed WC–CoCr coatings: An approach toward process maps. *J. Therm. Spray Technol.* **2014**, *23*, 1009–1018. [CrossRef]
20. Pulsford, J.; Venturi, F.; Pala, Z.; Kamnis, S.; Hussain, T. Application of HVOF WC–Co–Cr coatings on the internal surface of small cylinders: Effect of internal diameter on the wear resistance. *Wear* **2019**, *432*, 202965. [CrossRef]